Uptake of monohydric alcohols by liver: demonstration of a shared enzymic space

CARL A. GORESKY, ELLEN R. GORDON, AND GLEN G. BACH
McGill University Medical Clinic, Montreal General Hospital and Departments of Medicine, Physiology, and Mechanical Engineering, McGill University, Montreal, Quebec H3G 1A4, Canada

GORESKY, CARL A., ELLEN R. GORDON, AND GLEN G. BACH. *Uptake of monohydric alcohols by liver: demonstration of a shared enzymic space.* Am. J. Physiol. 244 (Gastrointest. Liver Physiol. 7): G198–G214, 1983.—Multiple-indicator dilution studies of the hepatic uptake of straight-chain C_1–C_5 monohydric alcohols were carried out in anesthetized dogs, with either no preceding or saturating infusions of ethanol, and at different steady-state levels for the C_2 experiments. Labeled red cells were utilized as a vascular reference, and labeled water was used as a second reference entering liver cells. Kinetic analysis of the data provided estimates of both an uptake rate constant and the space of distribution available to label. From the decrease in the uptake rate constant for labeled ethanol with bulk concentration, we calculated a maximal removal rate of 0.025 $\mu mol \cdot s^{-1} \cdot (ml\ liver\ water)^{-1}$ and a Michaelis constant (K_m) of 0.32 mM. Especially for the labeled C_3–C_5 alcohols, a space in excess of that available to water was found, and the bulk of this was dissipated by ethanol infusion. The increment, the "shared enzymic space," which varies with enzymic concentration and inversely with K_m, was used to calculate K_m values for the other alcohols.

in vivo uptake processes; liver uptake of methanol, ethanol, propanol, butanol, and pentanol; saturation effects in alcohol removal; alcohol dehydrogenase; ethanol displacement effects; enzyme competition effects in vivo; space effects at tracer concentration; heterogeneity of liver sinusoidal transit times; multiple-indicator dilution studies of alcohol uptake

---

IN THIS STUDY we examine two separate but connected phenomena: the kinetics of the removal of labeled ethanol in vivo, surveyed over a range of bulk plasma ethanol concentrations, and the hepatic uptake of the straight-chain labeled C_1–C_5 monohydric alcohols, examined at either radiochemical concentrations or after saturating infusions of bulk ethanol.

The liver is the main site of ethanol removal in vivo (32). Its removal kinetics saturate, and at plasma ethanol levels above 1–2 mM the rate of removal becomes constant (40). At these higher levels following load, plasma ethanol concentrations decrease in a linear fashion with time; at lower concentrations, plasma disappearance becomes exponential (the level declines at a rate proportional to the concentration in plasma rather than at a rate independent of the plasma concentration). Lundquist and Wolthers (31) originally suggested that these phenomena could be understood if Michaelis-Menten kinetics governed the disappearance of ethanol from blood, and much effort has been expended subsequently in order to obtain characteristic rate constants by analysis of peripheral ethanol-disappearance curves.

The structure of the liver is unique and must be considered when defining the manner in which this organ exerts its influence on the metabolic disposition of alcohol. It is composed of parallel sinusoids of similar length lined by endothelial cells with substantial gaps in their substance, a space of Disse (a functional extracellular space) beyond this, and plates of hepatocytes coadjacent to the space of Disse. The first potentially substantial barrier to the passage of materials into the liver is the liver cell membrane (15). Materials passing through this membrane gain access to the metabolic machinery in the liver cell. When a substrate is removed along the length of the sinusoid, a concentration profile in space is created, declining from input to terminal hepatic venule (1, 17). This concentration profile in space (with its corresponding input-output concentration difference) must be accounted for in any analysis of the way in which the liver removes substrates from the circulation.

Two different methods of approaching this problem have been developed. Keiding et al. (27) have examined the steady-state ethanol concentration differences across the liver over a range of concentrations spanning the effective Michaelis constant (K_m) in vivo and in the isolated perfused preparation. A steady-state equation was developed, with the assumption that the enzymic removal system was freely accessible to the alcohol; with this equation, maximal elimination rates (V_{max}) and K_m (the concentration of ethanol corresponding to half-maximal elimination) were obtained from sets of concentrations across the whole liver. The form displayed by the bulk extraction ratio was accounted for as a function of ethanol concentration (high at low concentrations and low at high concentrations). The remaining problems associated with this analysis are whether the liver cells are freely permeable to ethanol [if they are not, the theoretical basis for the analysis becomes questionable (19)] and the lack of consideration of the effects exerted by the heterogeneity of perfusion in the liver sinusoids in vivo, i.e., the difference between a single sinusoid and a whole liver.

The second approach that can be utilized is the multiple-indicator dilution technique (6, 17). With this particular design, a series of tracer experiments must again be carried out at different steady-state ethanol concentrations. With this approach and the use of both appropriate vascular reference tracers and extravascular space

0193-1857/83/0000-0000$01.50

reference tracers, the relative influence of the barrier at the parenchymal cell surface can be ascertained immediately, and the heterogeneity of perfusion must be dealt with as a primary experimental phenomenon in the data analysis. The results of this kind of analysis can be expected to complement the steady-state approach and, by their nature, to provide additional insight into the processes underlying the hepatic removal of ethanol.

We therefore carried out a series of multiple-indicator dilution tracer experiments with labeled ethanol in the livers of anesthetized dogs over a range of steady-state ethanol levels set by preceding infusion. These provided both a new general approach to this area and specific estimates of the parameters characterizing the enzymic process underlying the removal of ethanol by the liver.

The complementary set of experiments, designed to characterize the uptake of tracer straight-chain terminal monohydric alcohols, was carried out with a different aim in order to determine whether binding to the intracellular enzymic removal mechanism was visible in a fashion separable from a lipid-solubility phenomenon. The effect of intracellular binding on the apparent volume of distribution of tracers in vivo had previously only preliminary investigation. Two studies were carried out. Wolkoff et al. (43) examined the uptake of tracer bilirubin by the isolated perfused liver when the intracellular concentration of ligandin, the major intracellular binding protein for bilirubin, was manipulated pharmacologically. The volume of distribution in the liver accessible to the tracer bilirubin, as perceived from the plasma space, was found to increase in proportion to the increase in ligandin concentration. In these experiments no carrier bilirubin was added to the system. The binding sites on the ligandin, as demonstrated by the change in volume of distribution, were sensed by labeled bilirubin in radiochemical concentrations. If this low-concentration effect was a general phenomenon it might be expected that carrier-free tracers could be used to provide a relative index of the concentrations of proteins binding tracers in vivo. In contrast, at high levels of bulk concentration, a set of converse effects were found. In their multiple-indicator dilution exploration of the uptake of tracer palmitate by the liver, Goresky et al. (20) showed that the apparent intracellular space of distribution accessible to this tracer was substantially reduced by the preceding infusion of competitive inhibitors (as exemplified by α-bromopalmitate) and that this effect was paralleled by the inhibition of binding in supernatant cell fractions of labeled palmityl-CoA (which has an even higher affinity than palmitate) to the intracellular acceptor protein for free fatty acids, Z protein. The displacement effect at the binding sites on the Z protein correlated directly to the reduction in the volume of distribution in the liver, as perceived from the plasma space.

These two sets of observations suggested that the binding sites on enzymes provide an apparent extra space available to tracer, an enzymic space above and beyond the geometric tissue space, and that this apparent extra space could be diminished by increasing the concentration of unlabeled material (either the "mother substance" for the tracer or an analogous substance that exerts competitive effects at the binding site). This general hypothesis had not previously been examined systematically in an in vivo enzyme system. In an effort to find such an effect, we investigated the binding of the series of C_1–C_5 tracer straight-chain monohydric alcohols, both when no competing bulk ethanol was infused and after saturating infusions of bulk ethanol. We found an extra-space effect (a space of distribution available to the labeled alcohols larger than that available to labeled water) that increased markedly with chain length and that was almost ablated by ethanol infusion. Assuming that all of the alcohols are metabolized by a common enzymic mechanism (34), we were able to use both this experimentally measured increment in distribution space and the parameters calculated on the basis of the labeled ethanol explorations together with the results of the theoretical exploration of space effects at the level of the enzyme mechanism, outlined in the accompanying paper (19), in order to calculate Michaelis constants for the other alcohols in the series.

METHODS AND PROCEDURES

Multiple-indicator dilution studies. The rapid single-injection, multiple-indicator dilution technique is the basic experimental tool used in these studies (17). The experiments were carried out in 16- to 27-kg fasting mongrel dogs anesthetized with pentobarbital sodium. Food was removed from the animals for 14 h, but some of the animals still had either food in the stomach or milky chyle in intestinal lymphatics at the time of experimentation. Through an upper midline abdominal incision, catheters were placed in the main stem portal vein for injection and in the left main hepatic venous reservoir for the collection of hepatic venous samples, and the abdomen was closed. Two general protocols were utilized. Labeled ethanol experiments were carried out at different steady-state ethanol concentrations. To produce these, diluted ethanol was infused peripherally for 30 min before and during the multiple-indicator dilution experimental runs. The dosages utilized ranged up to 1 ml/kg body wt over 30 min. Additionally, the behavior of all of the labeled straight-chain terminal C_1–C_5 monohydric alcohols was investigated under two sets of circumstances. Multiple-indicator dilution studies were carried out either without preceding ethanol infusion or with the highest level of infusion used in the ethanol studies.

The injection mixture consisted of blood matched in hematocrit to that of the experimental animal, containing ^{51}Cr-labeled red cells (a vascular reference), tritiated water (a substance undergoing flow-limited distribution, which passes freely through the cell membranes of the hepatocytes), and the ^{14}C-labeled monohydric alcohol. To minimize the ethanol concentration difference between the injection mixture and the portal venous blood, in the infusion studies, the injection mixture was made up with plasma obtained from the portal venous catheter just before the experimental run. An aliquot of the injection mixture was stored in a closed container for later preparation of standards.

In each experiment, 1.8 ml of the injection mixture, previously incubated at 37°C, were injected as rapidly as possible through the portal venous catheter (injection

times of the order of 0.5 s were achieved), and serial anaerobic samples were collected from the hepatic vein over the next 30–45 s. The quantities of radioactivity injected for each experimental run were approximately 20 μCi for ^{51}Cr-labeled red cells, 100 μCi for tritiated water, and 20 μCi ^{14}C-labeled alcohol. The specific activities of the labeled alcohols ranged from 8 mCi/mmol for labeled methanol to 1 mCi/mmol for labeled pentanol. Gamma-ray spectrometry was used to determine ^{51}Cr activity in sample aliquots and appropriate standards; liquid scintillation counting was used to determine ^{3}H and ^{14}C activities in aliquots of the supernatants from ethanol-precipitated samples and standards. The samples were covered during preparation to guard against loss of volatile ^{14}C activity. To provide a basis for comparison between the materials injected, the outflow activity for each species was normalized by dividing it by the total injected. Effluent dilution curves were therefore expressed in terms of their outflow fraction per milliliter of blood versus time.

Measurement of ethanol levels. Arterial levels were measured when ethanol infusion was used. After sample collection, 5-ml whole blood was deproteinized with 2 N perchloric acid in sealed screw-capped tubes. The samples were centrifuged at 4°C to pack the precipitate, and the supernatant was analyzed for ethanol either by the enzymatic method of Bonnichsen (2) or by head-space gas chromatography. In the latter instance, 0.5 or 1.0 ml of the clear supernatant was placed in a precooled glass sample bottle designed for use with a Perkin-Elmer F-42 gas-liquid chromatograph equipped with a hydrogen flame detector. After preincubation at 60°C for 20 min, the head-space gas in these sample vials was injected automatically into the chromatograph. Separation was achieved on a 6-ft stainless steel column packed with 15% polyethylene glycol. The temperatures of the injection port, column, and detector were 150°C, 140°C, and 140°C, respectively. The helium flow was 50–60 ml/min. In each case a series of standard solutions of ethanol blanketing the range of observations were freshly prepared and treated in the same fashion as the unknown.

RESULTS

Forms of dilution curves in labeled ethanol experiments. Representative effluent dilution curves (expressed as outflow fraction per milliliter) for low-, intermediate-, and high-background, steady-state ethanol levels are illustrated in Fig. 1. The data are presented in a semilogarithmic format in the upper panels and in a rectilinear format in the lower panels. The labeled ethanol curve is related to the labeled water curve in each instance. On the semilogarithmic plots, the upslope of the labeled ethanol curve is initially close to that of the labeled water but with time progressively diverges, so that the peak of the ethanol curve is lower and (at lower concentrations) earlier than that of the labeled water curve, and the downslope of the labeled ethanol curve decays more rapidly than that of the labeled water curve. The whole labeled ethanol curve is contained within the labeled water curve and is related to it by a function, causing progressive divergence between the two curves with time. With increase in the concentration, the progressive divergence diminishes; in the extreme, when the underlying steady-state ethanol concentration is very high, it is clear that the form of the labeled ethanol curve converges on that of the labeled water curve. On the rectilinear plots the relation between the outflow recoveries of labeled ethanol and labeled water becomes obvious. At low ethanol levels the proportional removal of labeled

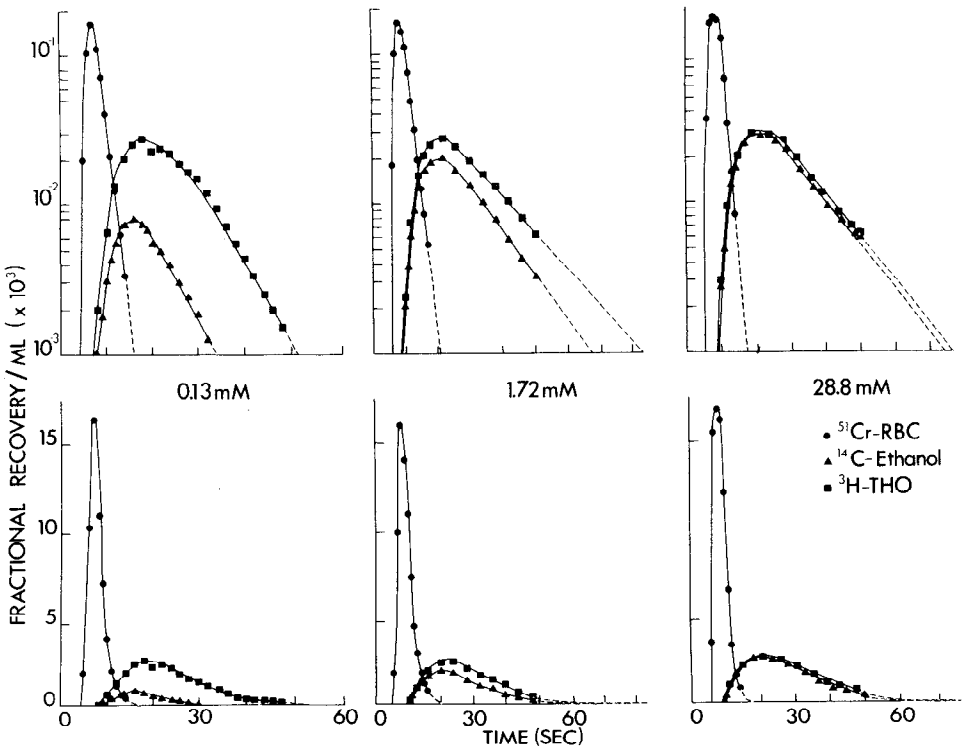

FIG. 1. Typical sets of outflow dilution curves. Values are plotted at midinterval of collection periods. *Upper panels:* dilution curves are plotted in a semilogarithmic fashion; *lower panels:* rectilinear coordinates. Data correspond to *experiments 1a, 8a,* and *12b* in Table 1. Time scale, both here and in later figures, is one in which input and collection catheter mean transit times have already been subtracted.

ethanol is very large; at high ethanol levels it becomes very small.

Goresky (15) has previously shown that labeled sucrose undergoes delayed wave flow-limited distribution into the extracellular space in the liver and labeled water undergoes flow-limited distribution into the total extravascular water space (a space including both Disse space and hepatocytes). When the two are included together in the injection bolus in an indicator dilution experiment, the labeled sucrose emerges substantially before the labeled water and, in comparison with the labeled water outflow fraction per milliliter versus time curve, its upslope is steeper, its peak is higher and earlier, and its downslope decays much more quickly. The areas under the two curves are of course equal. Substances entering the hepatocyte, for which the cell membrane is an appreciable barrier, exhibit an early component to their outflow dilution curve that is contained within the sucrose curve, with upslope and peak values occurring substantially earlier than those for labeled water (17, 21). The relation between the labeled water and labeled ethanol curves indicates that labeled water rather than labeled sucrose is the appropriate reference for the labeled ethanol curve, and the convergence of the labeled ethanol curve on the labeled water curve at high ethanol concentrations indicates that ethanol penetrates the cell membranes of the liver in the same fashion as labeled water, i.e., it is distributed into the hepatocytes in a flow-limited fashion. The form of the data thus indicates unequivocally that labeled ethanol penetrates the liver cell membranes freely and therefore that the assumption made by Keiding et al. (26) is correct.

Analysis of labeled ethanol outflow dilution curves. The labeled ethanol tracer dilution studies were carried out in a steady state with respect to ethanol, in which the ethanol concentration declines in each sinusoid from entrance to exit. Within a single dilution experiment the range of declines along the various sinusoids is too small, with respect to the range of concentrations that need exploration, in order to provide estimates of the characteristic parameters (maximal uptake rate of V_{tot}, expressed in micromoles per second per milliliter total space, and K_m) of the ethanol disposal system. Thus, although we have developed analytical expressions relating saturation effects and the characteristic parameters of the bulk removal system to tracer kinetics and these provide insight into both the behavior of the tracer ethanol removal system and the linkage between steady-state ethanol concentrations and tracer removal kinetics (19), the information obtained from a single dilution experiment does not appear to sweep across a wide enough concentration range to allow determination of characteristic parameters from the single experiment. To analyze the tracer dilution experiments, we have therefore assumed that the removal kinetics are linear across the range of concentrations encountered within a single experiment and have proceeded to analyze our experiments on this basis and to use the group data in toto to secure estimates of the characteristic parameters.

From the coincidence of the labeled ethanol and labeled water curves at high ethanol concentrations, it is reasonable to assume that the labeled ethanol propagates along the sinusoid in the same fashion as labeled water (in a delayed wave flow-limited fashion) and that metabolic uptake of tracer within the liver cell reduces the amount of tracer reaching the outflow in this wave. The two parameters describing this behavior, which can be derived from outflow dilution curves, are the tissue plus blood-to-blood space ratio, $(1 + \beta + \gamma + \theta)/(1 + \beta)$, describing the relative space of distribution available to tracer within the liver (this will include the enzymic space effect when this is present), and the uptake rate constant, $h_3\theta/(1 + \beta + \gamma + \theta)$, describing the rate of sequestration of tracer with the dimensions $ml \cdot s^{-1} \cdot (ml \text{ total space of distribution})^{-1}$ (19). The parameters β, γ, and θ represent the ratio of the accessible space in red cells, Disse space, and parenchymal cells to that available in plasma.

The relation between the outflow curves from the whole liver for labeled red cells and the completely recovered second-reference substance, labeled water, depends on the relation between the transit times of the large vessels and the transit times of the sinusoids. Because Goresky (15) has shown that the liver is described by the asymptotic extreme in which the large-vessel transit times are relatively uniform, we first exploited this relation. After a common large-vessel transit time, t_o, each point along the labeled water curve will have its transit time increased in relation to the labeled red cell curve by the space ratio $(1 + \beta + \gamma + \theta)/(1 + \beta)$; since the areas under the normalized curves are the same, its magnitude must be diminished by the inverse factor. The two parameters, t_o and the space ratio for labeled water, are obtained by transforming the labeled water curve in such a way as to reverse these effects, modifying the two parameters until superimposition of the adjusted labeled water curve on the labeled red cell curve is optimal, as judged by attainment of the least possible value for the sum of squares of the differences between the adjusted labeled water values and the observed red cell values (16). During venous outflow collection each sample is mechanically integrated over the sampling period, and hence each sample must be treated mathematically as if integrated over that interval. Therefore, although in our illustrations values are plotted at midinterval times, the function defined precisely is the cumulative outflow fraction per milliliter at end-interval times. We have therefore fitted a continuous three-point spline function to the experimental labeled water cumulative outflow values in order to provide a continuous interpolated function that can be manipulated as described above. The coefficient of variation of the final fit, CV, was utilized to characterize the goodness of that fit. This is defined as

$$CV = \sqrt{\Sigma(\hat{Y}_i - Y_i)^2/(n-2)}/(\Sigma\hat{Y}_i/N)$$

where $\hat{Y}_i$ is the calculated value and Y_i is the observed value. In these experiments the correspondence between the transformed labeled water curve and the labeled red cell curve was so good (avg CV of fit, 0.056) that the assumption underlying the transformation appears correct: the variation in transit times arises virtually entirely because of the heterogeneity of transit times in the exchanging hepatic sinusoidal system (23, 39). Then, with the t_o value derived above and the labeled water curve as

an initial template, we generated a set of reference curves corresponding to larger or smaller spaces of distribution and, with an estimate of the linearized rate constant for tracer alcohol removal, derived from these curves a set of calculated tracer alcohol curves. Fitting to the experimental alcohol curves by least squares was done to simultaneously optimize estimates for both the tissue plus blood-to-blood distribution ratio (which for ethanol is close to that for labeled water) and the linearized tracer removal rate constant. At the mechanical level, the new second-reference curve was generated from the spline-fitted labeled water curve with the new space ratio, and the calculated alcohol curve was generated by quadrature across 10 intervals within each sampling period as the product of the interpolated reference value and the negative exponential of the rate constant times the corresponding time of sinusoidal transit, $t - t_o$. The modeling approach to the process as a whole is outlined in the accompanying paper (19). For the group of ethanol experiments, the average relative coefficient of variation of the fit was 0.067. If the distribution of sinusoidal transit times (and its alternate projection, the heterogeneity of perfusion) were not taken into account, it would have been virtually impossible to account for the form of the labeled ethanol curve and the relative divergence with time of the tracer ethanol curves from the labeled water curves. The heterogeneity of sinusoidal transit times plays such a dominating role in shaping the outflow tracer ethanol curve that it must be considered in any scheme designed to describe the manner in which the whole liver removes ethanol.

Both the biological data characterizing the preparation and the derived parameters are given in Table 1: body weight; liver weight; hematocrit; hepatic perfusion rate; mean transit times for labeled red cells, labeled water, and labeled ethanol; steady-state ethanol concentrations at the time of the experiment; the relative outflow recoveries of tracer ethanol with respect to labeled water; the relative space ratios for labeled water and labeled ethanol; and the uptake rate constant for labeled ethanol. In analyzing the tracer experiments, the downslopes of the dilution curves were extrapolated on a semilogarithmic plot in order to exclude recirculation. The mean transit times were corrected for those of the input and collecting systems. Catheter distortion effects, which were expected to be small (22), were not removed from the data. In some cases both arterial and portal vein steady-state ethanol concentrations were measured. These were found to be virtually identical. The data in Table 1 show that the relative uptake rate constant for tracer ethanol varies systematically with the steady-state ethanol concentration in the manner expected: as the ethanol level rises the relative uptake rate constant decreases. A saturation phenomenon is occurring. The problem therefore became one of finding the dependence of the rate constant on the ethanol concentration and of defining how that relates to the removal mechanism at a more fundamental level.

Analysis of saturation effects. Fitting of the multiple-indicator dilution curves resulted in values for the two parameters, the total ethanol space-to-total water space ratio and the uptake rate constant for tracer ethanol. The values optimized for the first parameter, the total ethanol space-to-total water space ratio, are displayed in Fig. 2. The ethanol-to-water space ratio corresponded everywhere to unity, as expected, except when tracer ethanol experiments were carried out without preceding ethanol infusions. Then, when there was no carrier ethanol present, the average value for this ratio was 1.044. The discontinuity in tracer handling as the bulk

TABLE 1. *Experimental results and derived parameters for set of tracer ethanol experiments*

Expt No.	Body Wt, kg	Liver Wt, g	Hct, $ml \cdot ml^{-1}$	Hepatic Perfusion, $ml \cdot s^{-1} \cdot g^{-1}$	$\bar{t}_{RBC}$, s	$\bar{t}_{THO}$, s	$\bar{t}_{Eth}$, s	Ethanol Concn, $\mu mol \cdot ml^{-1}$	Tracer Ethanol Recovery	Space Ratio for THO	Space Ratio for Ethanol	Uptake Rate Constant for Ethanol, $ml \cdot s^{-1} \cdot ml^{-1}$
1a	16	457	0.33	0.0393	6.48	25.78	20.69	0.13	0.216	5.982	5.981	0.0554
1b	16	457	0.33	0.0353	6.30	30.39	26.25	0.58	0.431	6.386	6.399	0.0241
2a	18	510	0.36	0.0209	8.70	44.04	27.51	0.30	0.178	7.371	7.374	0.0466
3a	20	477	0.45	0.0255	6.52	28.78	22.13	0.67	0.316	7.264	7.264	0.0355
4a	20	866	0.28	0.0198	9.54	40.99	25.91	0.15	0.092	6.499	6.448	0.0533
5a	17	408	0.35	0.0109	18.31	63.01	40.66	0.78	0.124	4.482	4.483	0.0327
6a	18	318	0.40	0.0213	8.12	38.50	36.49	6.72	0.787	6.437	6.443	0.0059
7a	18	569	0.45	0.0172	7.48	58.83	24.81	0.29	0.084	8.899	8.899	0.0680
7b	18	569	0.45	0.0191	9.05	43.44	40.91	2.26	0.800	6.976	6.977	0.0049
8a	17	528	0.44	0.0256	6.44	27.70	25.22	1.72	0.660	5.986	6.033	0.0143
8b	17	528	0.44	0.0154	10.00	46.42	42.02	4.46	0.714	6.603	6.684	0.0072
9a	21	556	0.41	0.0127	8.42	57.88	55.70	15.67	0.877	9.854	9.854	0.0021
10a	18	329	0.45	0.0234	7.04	44.13	26.35	0.75	0.207	10.112	10.112	0.0369
10b	18	329	0.45	0.0227	8.19	37.86	24.46	0.87	0.293	7.671	7.630	0.0303
11a	17	408	0.49	0.0252	5.08	33.30	27.13	0.92	0.365	12.222	12.164	0.0242
11b	17	408	0.49	0.0227	5.91	27.88	25.84	0.74	0.485	6.540	6.548	0.0237
12a	15	448	0.42	0.0251	6.32	31.49	21.16	0	0.064	8.517	9.035	0.0963
12b	15	448	0.42	0.0288	6.02	29.51	28.03	28.80	0.964	6.353	6.355	0.0011
13a	22	652	0.36	0.0186	7.19	35.88	22.32	0	0.105	9.097	9.379	0.0748
13b	22	652	0.36	0.0249	5.81	32.43	32.05	34.80	0.966	10.481	10.499	0.0009
14a	21	714	0.44	0.0165	17.27	59.02	31.61	0	0.025	6.937	7.250	0.0808
15a	17	459	0.38	0.0216	11.14	47.75	29.65	0	0.054	6.915	7.186	0.0678
15b	17	459	0.38	0.0174	6.25	36.70	36.22	27.40	0.944	8.267	8.312	0.0014

$\bar{t}_{RBC}$, $\bar{t}_{THO}$, and $\bar{t}_{Eth}$, mean transit times for labeled red cells, labeled water, and labeled ethanol, respectively.

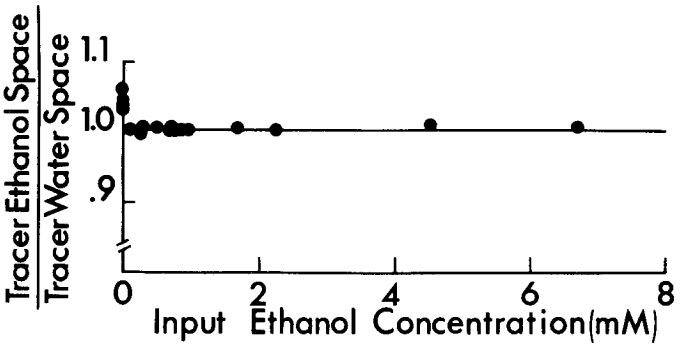

FIG. 2. Variation in ratio of total ethanol space to total water space with steady-state input ethanol concentration. All values approach closely to unity (line drawn across plot) except for those observations made with no preceding ethanol infusion.

ethanol concentration approaches zero appears to reflect the enzymic extra space effect and is examined later, along with the studies carried out with the other straight-chain monohydric alcohols in the absence of ethanol infusion.

The calculated uptake rate constants were found to diminish with increase in the input ethanol concentration, steeply over the lower concentration range and less steeply over the upper range. The problem that now presented was determining the parameters corresponding to the maximal ethanol removal rate and the Michaelis constant for the removal process. In the accompanying analysis (19) we show that the expected variation in the uptake rate constant with concentration is

$$\text{uptake rate constant} = \frac{V_{tot}}{(\hat{u} + K_m)} \qquad (1)$$

where V_{tot} is the maximal uptake rate for ethanol [μmol·s^{-1}·(ml total ethanol space)$^{-1}$], K_m is the Michaelis constant (μmol·ml^{-1} or mM), and $\hat{u}$ is the logarithmic average bulk ethanol concentration (μmol·ml^{-1} or mM). The logarithmic average $\hat{u}$ is defined by the equation

$$\hat{u} = \frac{u_o - u_L}{\ln u_o - \ln u_L} \qquad (2)$$

where u_o represents the common arterial and portal venous ethanol concentration and u_L represents the mixed hepatic venous ethanol concentration for the whole organ. Because in the accompanying analysis tracer outflow recoveries are shown to be proportional to bulk recoveries, the relative tracer ethanol outflow recoveries, based on the extrapolated tracer outflow curves, were utilized to calculate mixed venous outflow concentrations, and from the input and mixed venous outflow values logarithmic average concentrations were calculated. Our accompanying paper (19) and the analyses of Bass (1) and Keiding et al. (26, 27) indicate that $\hat{u}$ is an average that implicitly reflects the sinusoidal concentration profiles, exponential at low bulk concentrations and linear at high concentrations. When the removal rate constant is high at low absolute values of ethanol concentration, the value for the mixed venous $\hat{u}$ will be relatively substantially smaller than that for u_o; when the rate constant is low at high levels of ethanol concentration, the values for the mixed venous $\hat{u}$ will be much closer to those for u_o. In this system in which the steady-state profile is created immediately (because there are no barriers), the relative outflow tracer ethanol recovery at each point along the dilution curve will be directly related by the proportion of unlabeled ethanol surviving to the outflow with the particular kinetics characterizing that pathway. The mixed venous outflow concentration thus represents the average of effects over all paths. To ascertain that the logarithmic average calculated by use of this reflected the mean of the logarithmic averages calculated over all paths, we calculated the relative outflow logarithmic average concentrations along the tracer ethanol outflow curve, using corresponding tracer water values as appropriate input values for each point. These values were then summed over the total to give an average relative logarithmic concentration for all paths. The logarithmic average steady-state concentration corresponding to the tracer outflow was then calculated as the product of this value and the input steady-state ethanol concentration; the value was then compared with the value calculated more simply on the basis of the single value determined from the relative outflow recoveries of tracer ethanol and tracer water. The two are plotted against each other in Fig. 3. The values scatter very closely around the line of identity, and their correspondence indicates that it is appropriate to use the simpler approach to calculate the average $\hat{u}$ value on the basis of the single value obtained from the relative outflow recoveries of tracer ethanol and water.

Equation 1 merges together two approaches: the linear tracer analysis based on multiple-indicator dilution data (which takes into account the heterogeneities of flows within the liver) and the more formal analysis indicating that the logarithmic average (which takes into account the form of the concentration profile in cells and sinusoids) is the appropriate mean value to which to relate

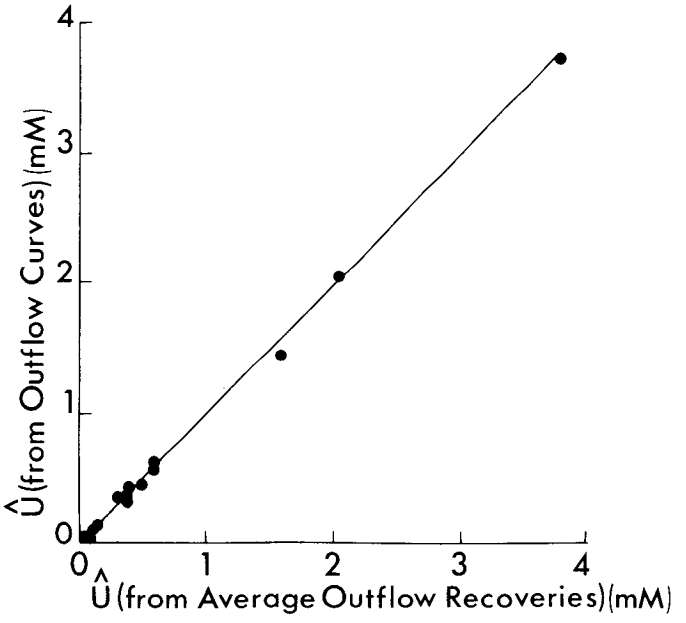

FIG. 3. Plot of $\hat{u}$, calculated from input ethanol concentration and summed logarithmic averages arising from tracer ethanol and tracer water curves, versus $\hat{u}$ values calculated simply from input ethanol concentration and relative outflow recoveries of labeled ethanol and labeled water. *Solid line:* line of identity. Four points corresponding to very high ethanol levels fall beyond right border of figure.

the linear analysis. In Fig. 4 we plotted the uptake rate constants as a function of the calculated logarithmic average ethanol concentrations. A line fitted by least squares was placed through the data, and the best-fit parameters, V_{tot} and K_m, resulting from this fit are listed in Table 2.

The data in Fig. 4 scatter uniformly about the least-squares line over the lower concentration range, but all points lie slightly above the line in the highest concentration range (some of the range is not illustrated). The deviation in the upper concentration range indicates that the removal rate is somewhat larger than would have been expected, on the basis of a single process saturating with the characteristics outlined by the least-squares fit. The data are compatible with the proposal of Lieber and Decarli (29) that at high ethanol concentrations an additional process (the microsomal ethanol-oxidizing system), with a much higher Michaelis constant than that of alcohol dehydrogenase, becomes involved in the removal process. Within the data set the determination of the removal rate constant becomes potentially susceptible to greater relative error at high ethanol concentrations when the difference between the labeled ethanol and reference-labeled water curves becomes very small (10); we therefore did not use our high-concentration data to quantitate this second pathway, even though Johansen and Keiding (25) indicated how the problem might be approached.

Effect of removal process on relative recovery of tracer ethanol and on form of tracer ethanol dilution curve. The relative recovery of tracer ethanol is plotted as a function of the labeled ethanol removal rate constant in the upper panel of Fig. 5. The relative outflow recovery decreases systematically as the ethanol removal rate constant increases. Minimal outflow recoveries are found for those experiments in which no infusion was utilized. The extraction across the liver is never complete, however, even when tracer was injected with no carrier ethanol present in the system. The ratio of the mean transit time for outflow tracer ethanol to that for outflow tracer water is plotted as a function of the ethanol removal rate constant in the lower panel of Fig. 5. For those experiments in which the tracer water is the appropriate reference (i.e., for all experiments except those with no ethanol infusion), the tracer ethanol was expected to have the same transit time as the tracer water, unless the removal process reshaped the curve as a consequence of heterogeneity of perfusion or transit times (23, 38). The ratio of the labeled outflow ethanol to labeled water transit times provides an index of the degree to which the tracer ethanol outflow dilution curves are reshaped. The illustration demonstrates a major and systematic decrease in this ratio with increase in the ethanol removal rate constant [as would have been expected from the forms of the curves in Fig. 1 and the analysis outlined in the accompanying paper (19)].

Changes in relative forms of outflow curves across series from methanol to pentanol. In the sequence from methanol to pentanol, the forms of the outflow tracer alcohol curves relative to those for tracer water change progressively as the chain length for the alcohol in-

TABLE 2. *Fitted parameter values*

Data Utilized	V_{tot}, $\mu mol \cdot s^{-1} \cdot ml^{-1}$	K_m, $\mu mol \cdot ml^{-1}$	SE of Fit, $ml \cdot s^{-1} \cdot ml^{-1}$
Logarithmic average concn	0.025	0.32	0.0071

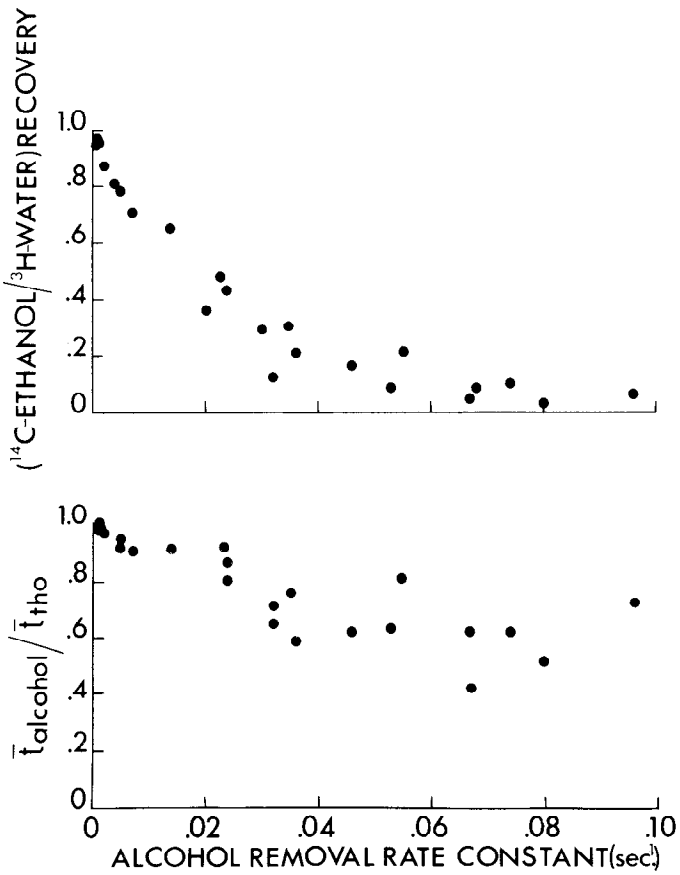

FIG. 5. Outflow recovery of tracer ethanol relative to that of tracer water and ratio of mean transit time of tracer ethanol to that of labeled water as a function of ethanol removal rate constant.

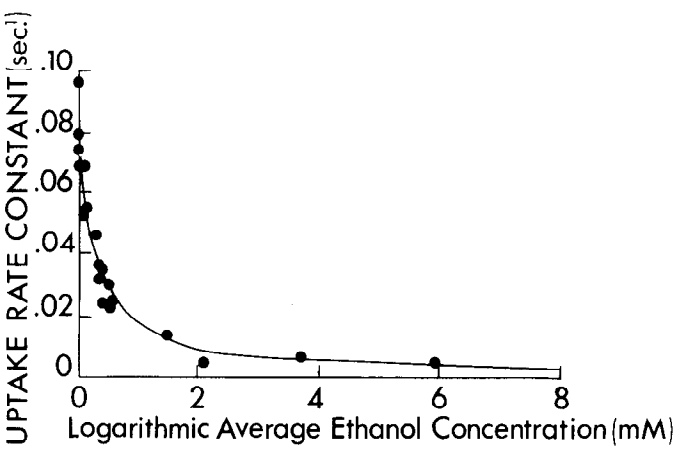

FIG. 4. Change in tracer uptake rate constant with underlying concentration of ethanol. Tracer ethanol uptake rate constant is plotted as a function of logarithmic average ethanol concentration. Four experimental runs with very high ethanol concentrations fall beyond right boundary of figure. Present expanded ethanol concentration was chosen to emphasize change in uptake rate constant with ethanol concentration across lower concentration range.

creases, both when the tracer alcohol is given with no preceding infusion of alcohol and when a large amount of ethanol has previously been infused. Loading with any of the short-chain monohydric alcohols other than ethanol would have produced potentially difficult reactions. Methanol infusion would have produced methanol poisoning. Infusion of only very small amounts of propanol and butanol results in massive hemolysis, and the solubility of pentanol in aqueous solution is limited. The only short-chain alcohol appropriate for infusion in the doses needed for the exploration of saturation effects is ethanol.

The results of an experiment in which labeled methanol was used with no preceding ethanol infusion are illustrated in Fig. 6. The labeled red cell and water curves resemble those shown earlier in the labeled ethanol studies. The labeled methanol curve is very closely related to the labeled water curve. It deviates from it to a minor extent by virtue of a small-scale sequestration of tracer by the liver. It is clear in this instance that the labeled water curve is the appropriate reference for the labeled methanol (i.e., it represents the form the labeled methanol curve would have had if there had been no metabolic sequestration of label). The infusion of ethanol results in reversion of the methanol curve toward the labeled water curve. Because the original deviation was small and the new curve is not very different, the findings are not illustrated.

Labeled ethanol curves are illustrated in Fig. 7. When there was no preceding ethanol infusion, massive uptake of the tracer occurred. Only a very small proportion of the label emerged at the outflow. In this case the labeled ethanol curve is close to the labeled water curve in its initial upslope and then progressively diverges from it, so that its peak is much lower and earlier than that for labeled water and its downslope decays more rapidly. Inspection of the curves would lead one to believe that the appropriate reference for the tracer ethanol curves would have a space of distribution close to that for labeled water. When high-load ethanol was infused, uptake of labeled ethanol was massively suppressed. The labeled ethanol curve closely approached that for labeled water. The labeled water curve is now obviously the appropriate reference for the labeled ethanol curve.

The propanol curves, illustrated in Fig. 8, show a departure from the preceding pattern. When there was preceding ethanol infusion, the labeled propanol emerged substantially later than the labeled water curve. Its outflow fraction per milliliter rose to a much later and lower peak. The curve is quite obviously no longer closely related to the labeled water curve. Its appropriate reference curve would have a volume of distribution substantially larger than that available to labeled water. After the infusion of an ethanol load, the labeled propanol emerged much earlier (just after the labeled water), its outflow fraction per milliliter rose to a peak just below and slightly later than that for labeled water, and the two curves converged on their downslopes. The appropriate reference for the labeled propanol curve now moves to a position substantially closer to that for labeled water.

The labeled butanol shows a pattern similar to that found with propanol. Representative outflow profiles are illustrated in Fig. 9. When there was no preceding ethanol infusion, the labeled butanol emerged substantially later than the labeled water, its outflow fraction per milliliter again reaching a later and lower peak, and it crossed the labeled water curve on its downslope. The space of distribution for the appropriate reference was substantially larger than that for labeled water. After a loading ethanol infusion, the labeled butanol emerged slightly delayed with respect to the labeled water, and its outflow fraction per milliliter then rose more or less in parallel with the labeled water curve. From the form of the curves after alcohol loading, the appropriate reference for the labeled butanol was expected to approach that of a substance with a space of distribution slightly larger than that for labeled water.

With labeled pentanol the same kind of pattern is again seen. The findings when there was no preceding ethanol infusion are illustrated in Fig. 10. The labeled pentanol emerged appreciably later than the labeled water. Its outflow fraction per milliliter rose substantially slower than that for labeled water to reach a peak that in this case was so delayed that it related to the down-

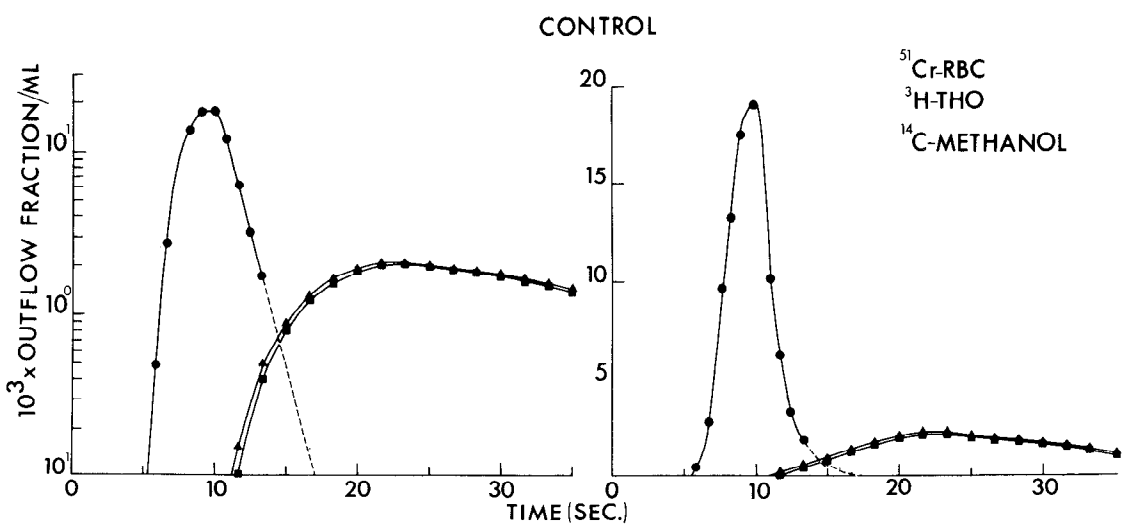

FIG. 6. A typical set of outflow dilution curves from a labeled methanol experiment carried out without a bulk ethanol infusion.

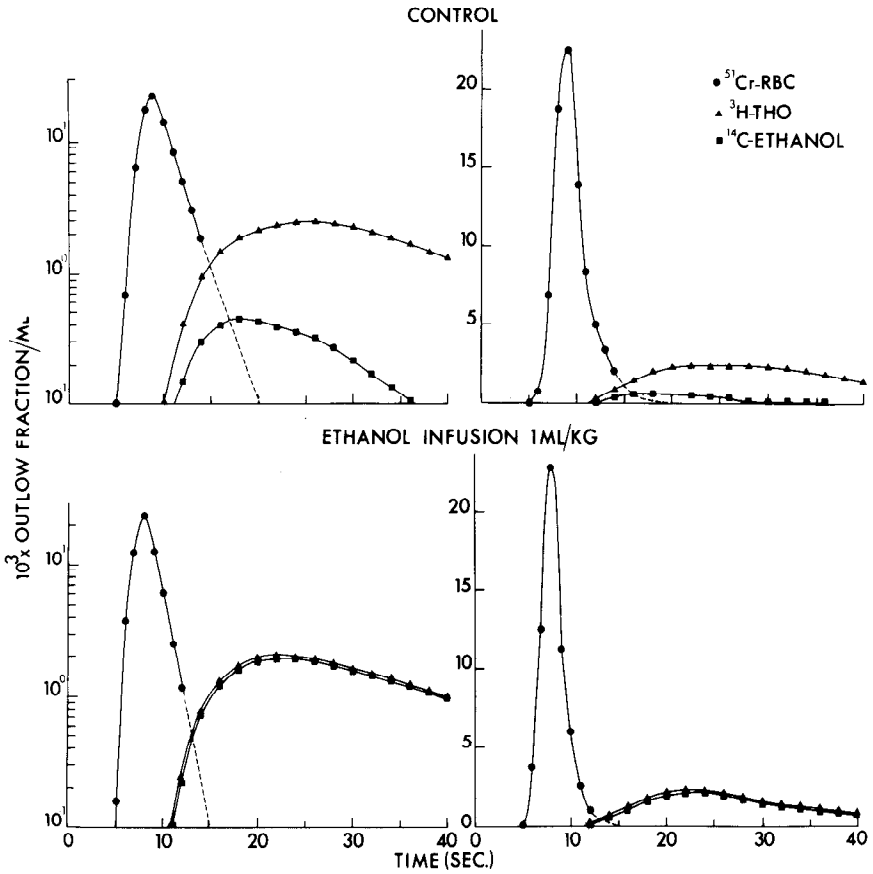

FIG. 7. Typical sets of outflow tracer dilution curves from labeled ethanol experiments without (control) and with preceding and concurrent bulk ethanol infusion.

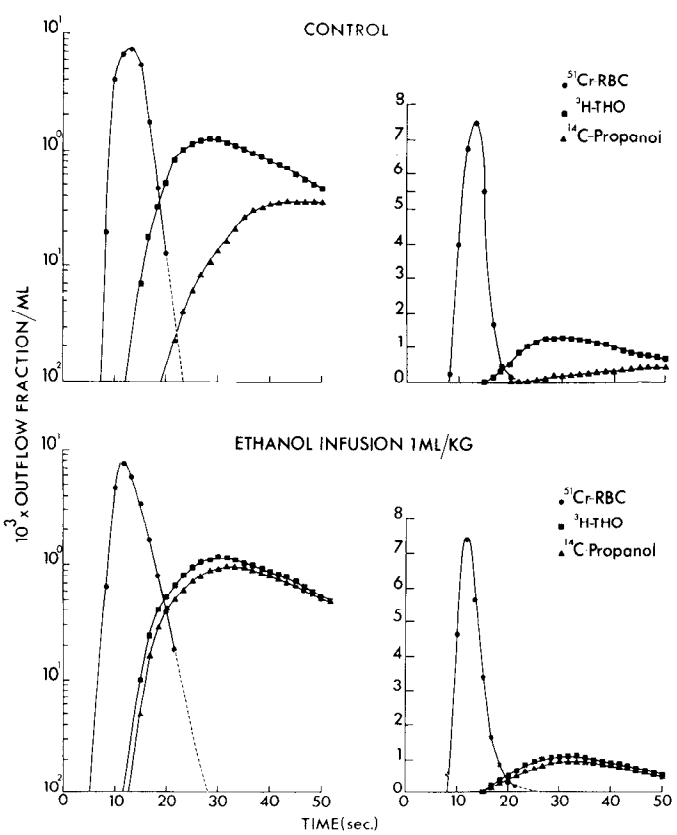

FIG. 8. Outflow tracer dilution curves from labeled propanol experiments without (control) and with preceding and concurrent bulk ethanol infusion.

slope of the labeled water curve. The space of distribution for its appropriate reference was substantially larger than that for labeled water. The cost of labeled pentanol was high, and so in this instance the experiment was not repeated after a preceding ethanol infusion. A reversion in the form of the outflow curve toward that for labeled water, similar to that observed for butanol, would have been expected.

Analysis of monohydric alcohol experiments performed without and with high-level ethanol infusions. The set of procedures utilized for the analysis of the ethanol experiments were general in design and therefore were also utilized for the analysis of this second set of experiments. The fitting procedures provide optimized estimates of the tissue-to-blood space ratio for labeled water, the tissue-to-blood space ratio for the labeled monohydric alcohol examined, and an uptake rate constant describing the relative rate of sequestration of tracer with the dimensions $ml \cdot s^{-1} \cdot (ml\ total\ space\ of\ distribution)^{-1}$. A calculated labeled alcohol curve was generated in the analysis process and fitted to the experimental data as closely as possible with a least-squares criterion. For this set of data, the fit was quite good (avg relative CV of fit, 0.057). The tissue-to-blood space ratio for the alcohol also provided a parameter with which to generate the outflow profile for the appropriate reference for the tracer alcohol (the form its outflow curve would have had if there had been no uptake).

The calculated appropriate reference curves and the effect of the uptake process are depicted in Figs. 11–15 for the experiments already illustrated in Figures 6–10.

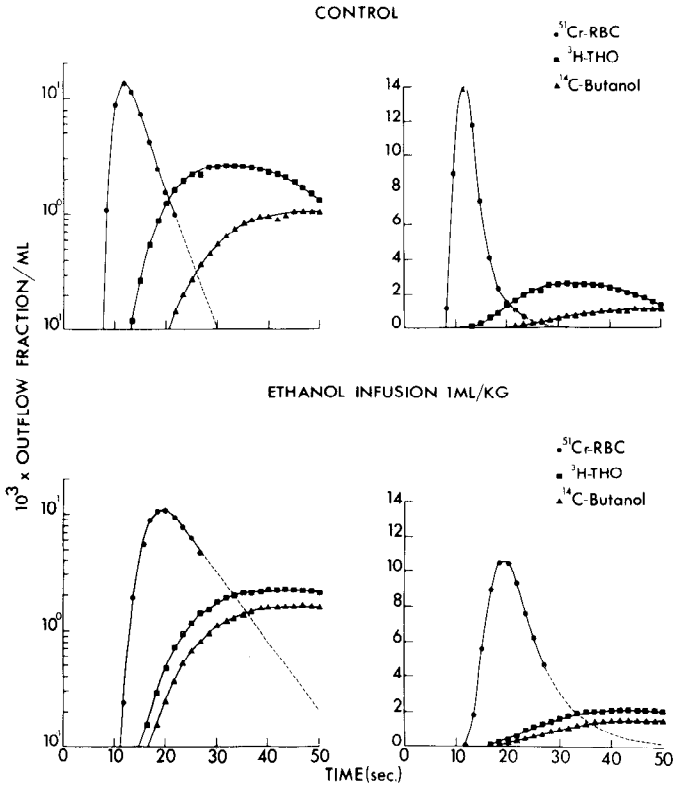

FIG. 9. Outflow tracer dilution curves from labeled butanol experiments.

In Fig. 11 it is obvious that, as expected, the appropriate reference for the tracer methanol is not perceptibly different from the outflow profile for the labeled water. The uptake effect, the area between the two curves, is shaded. In Fig. 12 labeled ethanol experiments both without and with previous high-level bulk ethanol infusion are illustrated. In the experiment shown in the left-hand panel, in which tracer was used without previous ethanol infusion, it can be seen that the appropriate reference (the dashed line) had a space of distribution slightly larger than that for labeled water. The uptake effect, the area between this curve and that for the labeled ethanol, was shaded. It is evident that uptake of the tracer ethanol was massive. After the steady infusion of bulk ethanol, the uptake of tracer was inhibited. The tracer water curve became the appropriate reference for the labeled ethanol, and the uptake effect, the area between the two curves, became quite small.

For the longer-chain alcohols the reference curves are quite different from those for labeled water when no preceding infusion of ethanol was utilized. Figure 13 depicts the appropriate reference and the uptake effect for labeled propanol, both without and with infusion of bulk ethanol. When no ethanol was infused, the appropriate reference for the labeled propanol curve had a space of distribution substantially larger than that for labeled water, and the uptake effect (the shaded areas, corresponding to the proportion of tracer propanol removed during passage through the liver) was substantially smaller than with tracer ethanol. After an infusion of bulk ethanol the appropriate reference curve for the tracer propanol curve approached that for the labeled water but did not become coincident with it. The uptake effect was also substantially reduced. For labeled butanol an essentially similar set of phenomena are displayed in Fig. 14. After bulk ethanol infusion, the reference curve for the labeled butanol did not approach that for labeled water so closely and the uptake effect became small. The space of distribution after the bulk ethanol infusion, relative to that for labeled water, was somewhat larger than in the case of labeled propanol. The analysis of a labeled pentanol experiment is displayed in Fig. 15 for the case in which no preceding bulk ethanol infusion was used. The labeled reference again had a substantially larger space of distribution than that for labeled water, and the uptake effect (the shaded area) became relatively small.

Parameter estimates arising from analysis of set of tracer monohydric alcohol outflow curves: effect of ethanol infusion. The biological data characterizing the

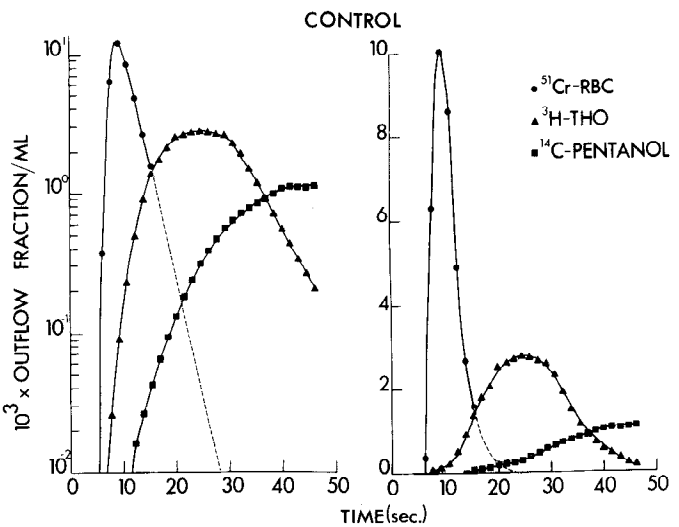

FIG. 10. Outflow dilution curves from a labeled pentanol experiment with no bulk ethanol infusion.

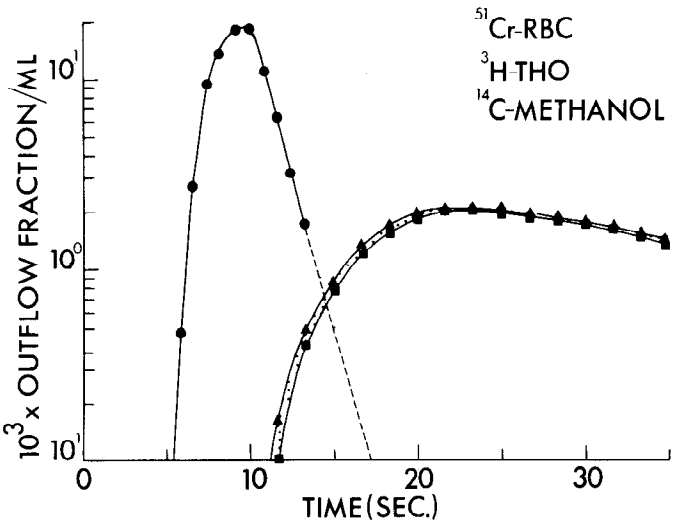

FIG. 11. Uptake effect in a labeled methanol experiment. In this case appropriate reference curve corresponds to labeled water curve. Shaded area between labeled water and labeled methanol curves represents effect of uptake process. Experiment is same as that illustrated in Fig. 6.

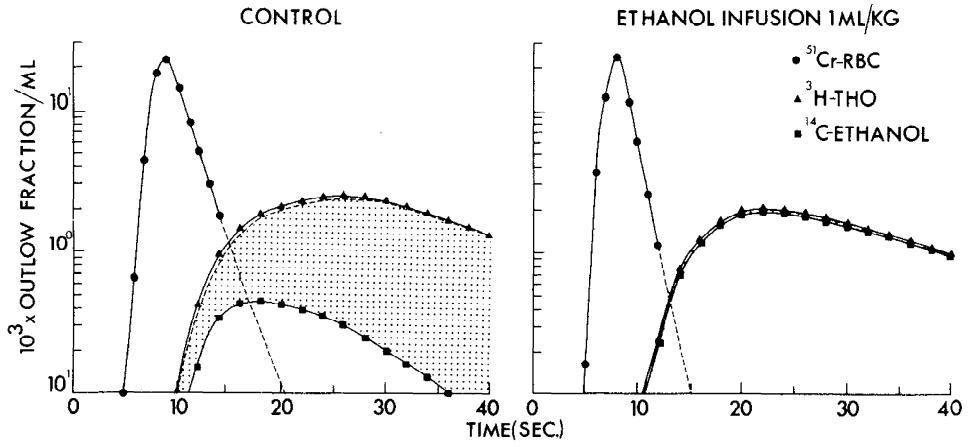

FIG. 12. Results of analysis of ethanol experiments illustrated in Fig. 7, without (*left-hand panel*) and with (*right-hand panel*) bulk ethanol infusion. Appropriate reference is illustrated as a *dashed line* in left-hand panel. It is labeled water curve in right-hand panel. Uptake effect, area between appropriate reference curve and labeled ethanol curve, is shaded in each panel.

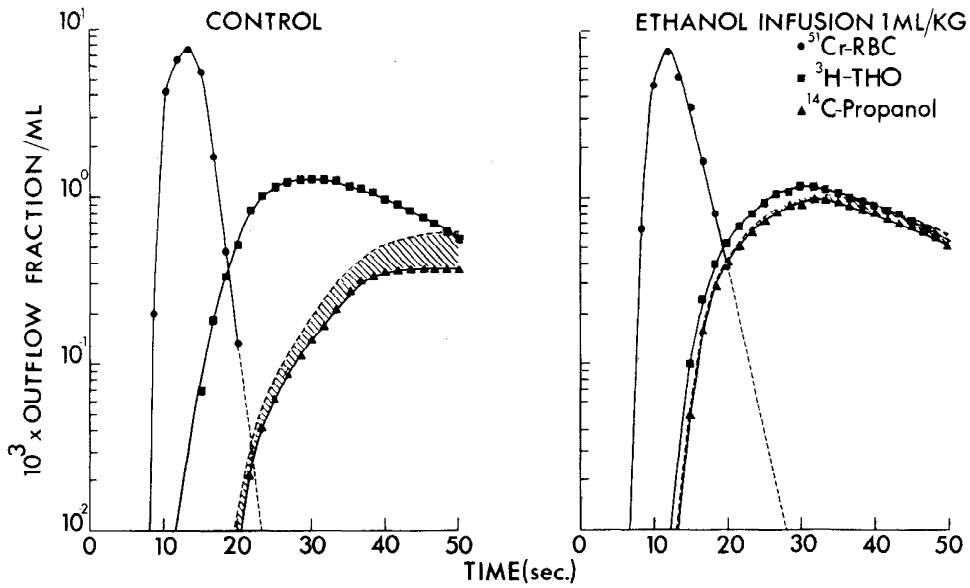

FIG. 13. Results of analysis of propanol experiments illustrated in Fig. 8, without (*left-hand panel*) and with (*right-hand panel*) bulk ethanol infusion. Appropriate reference is illustrated as a *dashed line* in each panel. Uptake effect, area between appropriate reference curve and labeled propanol curve, is shaded.

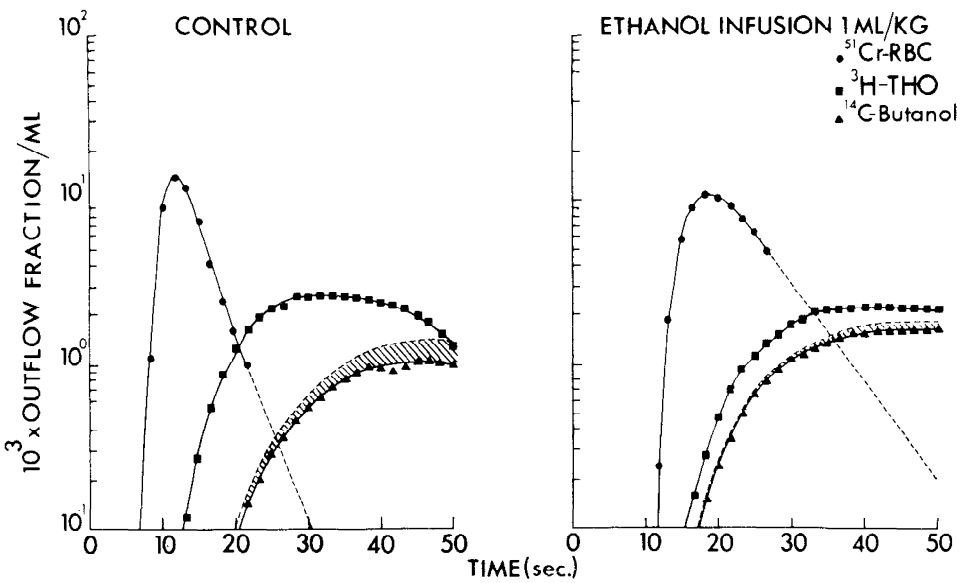

FIG. 14. Results of analysis of butanol experiments illustrated in Fig. 9, without (*left-hand panel*) and with (*right-hand panel*) bulk ethanol infusion. Appropriate reference is again illustrated as a *dashed line*. Uptake effect is shown as a shaded area.

preparations and the derived parameters are listed in Table 3: body weight; liver weight; hematocrit; hepatic perfusion rate; mean transit times for red cells and labeled water; the relative ethanol concentration; the relative space ratios for labeled water and the monohydric alcohol; the ratio of the space ratio for labeled alcohol to that for the labeled water; an estimated value for the ratio of cell space available to the labeled alcohol to cell

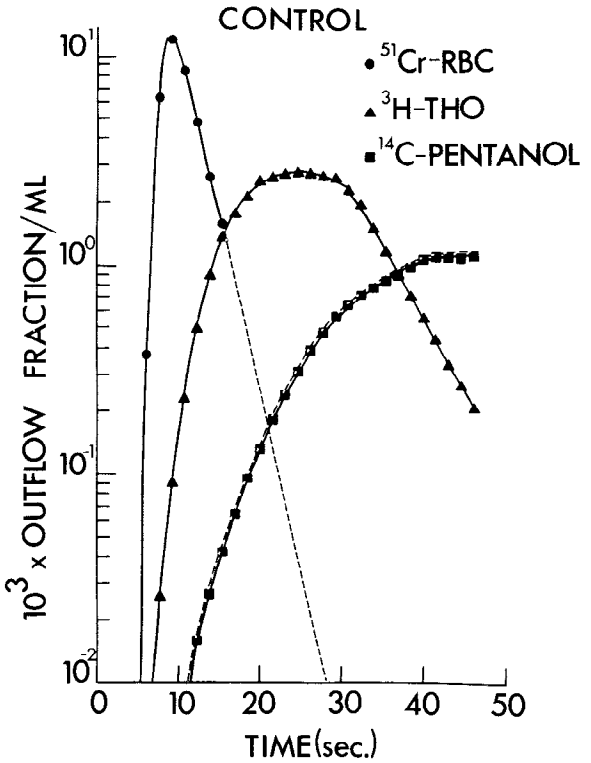

FIG. 15. Result of analysis of pentanol experiment illustrated in Fig. 10, in which there was no preceding ethanol infusion. Appropriate reference curve is again illustrated by a *dashed line*, which in this case is so close to pentanol curve that there is no room for shading area in between.

space available to labeled water; and the uptake rate constant for the labeled alcohol. The no-infusion and high-infusion ethanol data are repeated to provide for easy comparison with the other monohydric alcohols. The two important parameters arising from the fitting procedure are the ratio of the alcohol space to the water space and the uptake rate constant for tracer. After high-dose ethanol infusion, the expected pattern of change emerges with each alcohol: the alcohol-to-water space ratio decreases toward unity and the uptake rate constant decreases.

Relation between experimental observations and enzymic space effect. It is appropriate to first examine the data for ethanol because tracer uptake was examined over a wide range of underlying bulk ethanol concentrations, and the K_m value obtained is expected to be reasonably accurate. In the present set of experiments, we also obtained values for the ratio of the monohydric alcohol space to the water space. In the accompanying theoretical work (19), we have shown that the magnitude of the ratio of the alcohol space to the water space is in general

$$\frac{(1 + \beta + \gamma + \theta'\{1 + e_T/[u + K_m]\})}{(1 + \beta + \gamma + \theta)}$$

where θ' is the parenchymal-to-sinusoidal plasma space ratio for the alcohol in the absence of an enzymic effect, and is distinct from the ratio θ for water, e_T is the concentration of enzymic binding sites, and u is the concentration of bulk material; thus, in the absence of bulk infusion ($u \rightarrow 0$), the ratio becomes

$$\frac{(1 + \beta + \gamma + \theta'\{1 + e_T/K_m\})}{(1 + \beta + \gamma + \theta)}$$

and, after high-level bulk infusion ($u \rightarrow \infty$), the ratio becomes

$$(1 + \beta + \gamma + \theta')/(1 + \beta + \gamma + \theta)$$

Because our data indicate that $\theta' = \theta$ for labeled ethanol, we find, as a consequence, that the opportunity to find e_T presents. The value for β, the red cell water-to-plasma water ratio, can be calculated from the hematocrit (Hct). It is 0.70 Hct/(0.94 [1 − Hct]), where the values 0.70 and 0.94 represent the water contents of red cells and plasma, respectively, with the dimensions $ml \cdot ml^{-1}$. The value for γ, the ratio of available Disse space to sinusoidal plasma space, should be that for a low-molecular-weight substance, one for which there will be no exclusion effect modifying its penetration into the space of Disse (15). Since no label was present in the injection mixture that would have provided a direct estimate of γ, the ratio of the accessible extravascular extracellular volume to the sinusoidal plasma volume for the labeled alcohol or labeled water, this parameter was estimated in the following manner. The value for γ was assumed to be equal to the average found for labeled sucrose, a low-molecular-weight substance that does not penetrate liver cells, in a representative set of experiments [avg value of 1.03 (17) at an average hematocrit of 0.33]. Where the hematocrit varied from this value, the estimated value of γ was modified appropriately. Then, knowing the values of β and γ, we calculated the value of θ for labeled water and that of $\theta'(1 + e_T/\{u + K_m\})/\theta$ for the labeled alcohol for the two extremes ($u \rightarrow 0$ and $u \rightarrow \infty$). The values for $\theta'(1 + e_T/\{u + K_m\})/\theta$ are listed in Table 3 for the two extremes.

Because, in the case of ethanol, the value for the K_m is known to be 0.32 $\mu mol \cdot ml^{-1}$, the value for e_T can be approximated from the tabulated average value, 1.057, for the $u \rightarrow 0$ case $(1 + e_T/K_m)$. From this, e_T is estimated to be 0.019 $\mu mol \cdot ml^{-1}$ in terms of its ethanol-binding sites. Then, if we make the reasonable assumption that the same enzyme, alcohol dehydrogenase, is responsible for binding the other straight-chain monohydric alcohols, especially over the low concentration range, and if we also assume that $\theta' = \theta$, it becomes possible with knowledge of e_T to calculate a K_m value for the other alcohols from the values that we have tabulated for the $u \rightarrow 0$ extreme $(1 + e_T/K_m)$. The K_m estimates are listed in the middle column of Table 4.

The change in the distribution volumes for the alcohols and in the estimated values for $\theta'(1 + e_T/\{u + K_m\})/\theta$ after the high-dose ethanol infusion indicates that at the very high ethanol levels, when the ratio will be expected to approach θ'/θ, a small increment in the extravascular space available to the monohydric straight-chain alcohols above the water space remains, and this increment increases with the chain length of the alcohol. If we assume that this is simply a solubility phenomenon (that the alcohol dissolves in the lipid phases of the cell, which are virtually inaccessible to tracer water), the estimated values for K_m should be corrected for this phenomenon. We have therefore carried out this correction and listed the

TABLE 3. *Experimental results and parameters derived from tracer monohydric alcohol experiments both without and with high-level ethanol infusion*

Expt. No.	Body Wt, kg	Liver Wt, g	Hct, ml·ml^{-1}	Hepatic Perfusion, ml·s^{-1}·g^{-1}	t_{RBC} s	t_{THO} s	Relative Ethanol Concn	Space Ratio for THO	Space Ratio for Alc	Alc Space/ Water Space	Estimated Alc Cell Space/ Water Cell Space	Uptake Rate Constant for Alc, ml·s^{-1}·ml^{-1}
						Methanol experiments						
16a	17	543	0.37	0.0255	8.44	42.42	Zero	6.893	6.894	1.0001	1.0004	0.0024
16b	17	543	0.37	0.0234	12.63	49.74	High	4.951	4.953	1.0004	1.0006	0.0013
17a	15	506	0.30	0.0274	6.37	33.29	Zero	8.135	8.137	1.0002	1.0003	0.0025
17b	15	506	0.30	0.0463	5.75	28.24	High	7.109	7.155	1.0065	1.0085	0.0010
Mean							Zero			1.00015	1.00035	0.00245
±SD										±0.00007	±0.00007	±0.00007
							High			1.0034	1.0045	0.00115
										±0.0043	±0.0056	±0.00021
						Ethanol experiments						
12a	15	448	0.42	0.0251	6.32	31.49	Zero	8.517	9.035	1.0608	1.0770	0.0963
12b	15	448	0.42	0.0288	6.02	29.51	High	6.353	6.355	1.0003	1.0004	0.0011
13a	22	652	0.36	0.0186	7.19	35.88	Zero	9.097	9.379	1.0310	1.0386	0.0748
13b	22	652	0.36	0.0249	5.81	32.43	High	10.481	10.499	1.0017	1.0021	0.0009
14a	21	714	0.44	0.0165	17.27	59.02	Zero	6.937	7.250	1.0451	1.0609	0.0803
15a	17	459	0.38	0.0216	11.14	47.75	Zero	6.915	7.186	1.0392	1.0528	0.0078
15b	17	459	0.38	0.0174	6.25	36.70	High	8.267	8.312	1.0054	1.0071	0.0014
Mean							Zero			1.0440	1.0573	0.0799
±SD										±0.0126	±0.0160	±0.0121
							High			1.0025	1.0036	0.00113
										±0.0026	±0.0042	±0.00025
						Propanol experiments						
18a	27	567	0.47	0.0198	12.11	45.76	Zero	7.012	15.805	2.254	2.6832	0.00543
18b	27	567	0.47	0.0211	11.04	48.38	High	9.221	9.412	1.021	1.0257	0.00054
19a	19	790	0.33	0.0306	12.95	44.03	Zero	6.162	12.552	2.037	2.4555	0.00999
19b	19	408	0.33	0.0299	12.33	46.96	High	6.757	7.325	1.084	1.1140	0.00251
20a	18		0.42	0.0183	9.33	37.52	Zero	10.814	35.600	3.292	3.7472	0.00034
20b	18	408	0.42	0.0265	9.38	39.17	High	12.333	12.948	1.050	1.0583	0.00150
21a	12	466	0.33	0.0332	10.57	37.15	Zero	7.823	20.848	2.665	3.1526	0.00036
22a	18	534	0.54	0.0433	11.89	28.22	Zero	3.849	8.428	2.190	3.8331	0.00269
23a	14	398	0.38	0.0472	10.17	30.67	Zero	5.918	17.718	2.994	3.8536	0.00030
24a	14	436	0.49	0.0280	11.72	49.31	High	8.909	9.322	1.046	1.0582	0.00064
25a	16	472	0.20	0.0510	9.18	21.86	High	3.665	3.807	1.038	1.0732	0.00217
Mean							Zero			2.572	3.2875	0.00319
±SD										±0.498	±0.6173	±0.00390
							High			1.048	1.0659	0.00147
										±0.023	±0.0320	±0.00088
						Butanol experiments						
26a	17	555	0.26	0.0257	10.07	30.77	Zero	5.285	9.509	1.799	2.1975	0.00741
27a	20	461	0.44	0.0238	12.61	51.01	High	8.279	9.140	1.104	1.1328	0.00364
28a	15	479	0.37	0.0213	13.57	45.93	High	6.332	7.057	1.115	1.1436	0.01277
29a	14	517	0.38	0.0140	22.44	63.49	High	4.726	5.740	1.215	1.3445	0.0256
30a	17	367	0.50	0.0364	14.85	58.75	Zero	7.264	17.201	2.068	2.8217	0.01921
31a	15	500	0.41	0.0193	9.13	38.11	Zero	9.781	17.851	1.825	2.0098	0.02239
Mean							Zero			1.997	2.3430	0.01634
±SD										±0.321	±0.4251	±0.00789
							High			1.145	1.2070	0.00632
										±0.061	±0.1192	±0.00561
						Pentanol experiment						
32a	15	336	0.25	0.0486	10.32	26.70	Zero	4.49	10.426	2.360	3.2594	0.00108

TABLE 4. *Estimated K_m values with and without corrections for apparent lipid solubility effect*

	Estimated K_m, μmol·ml^{-1}	Corrected K_m, μmol·ml^{-1}
Methanol	54	54
Ethanol	0.33	0.33
Propanol	0.0083	0.0091
Butanol	0.0141	0.0201
Pentanol	0.0084	

corrected K_m values in the right-hand column of Table 4. The finding of a small extra space dependent on an apparent solubility effect is not unique. It has previously been observed both in kidney and in lung (33).

DISCUSSION

Description of ethanol uptake kinetics. The success of the present analysis of uptake kinetics at the level of single-dilution curves presents a striking example of the

TABLE 5. *Comparative K_m values of alcohol dehydrogenase for straight-chain monohydric alcohols*

Investigator	Source	Species	Conditions	K_m Values, mM				
				Methanol	Ethanol	Propanol	Butanol	Pentanol
Present studies	Liver in situ	Dog	In vivo	54	0.33	0.0091	0.0201	~0.01
Feytmans & Leighton (9)	Purified enzyme	Rat	pH 7.0, 30°C	340	0.26			
Tsai (42)	Purified enzyme	Horse	pH 9.0, 30°C		0.7	0.3	0.08	0.06
Lange et al. (28)	Purified enzyme	Human	pH 10.0, 25°C	2.9	2.7	0.40	0.033	0.040
Pietruszko et al. (35)	Purified enzyme	Horse	pH 7.5, 25°C		0.76	0.27	0.25	
Pietruszko et al. (35)	Purified enzyme	Human	pH 7.5, 25°C		0.40	0.10	0.14	
Pietruszko (34)	Purified enzyme	Horse	pH 7.0, 25°C			0.06	0.01	

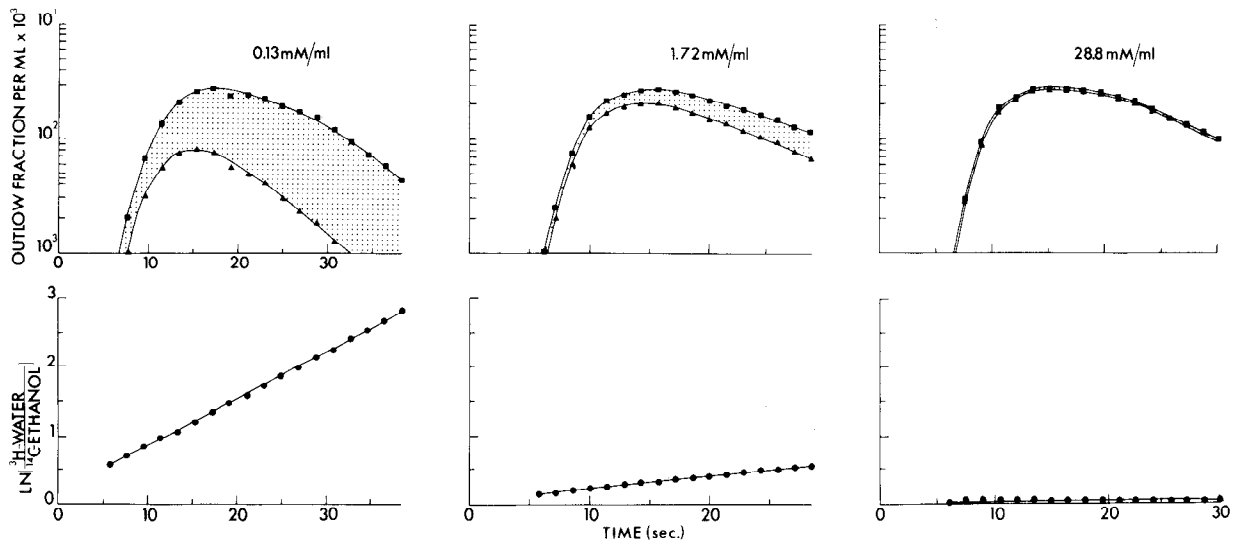

FIG. 16. Effects of uptake and a simple way of characterizing uptake rate constant. *Upper panel:* because labeled water curve is appropriate reference for labeled ethanol curve, *shaded area* represents effect of uptake process. *Lower panel:* slope of plot provides a direct estimate of ethanol removal rate constant. Data plotted are same as those of experiments illustrated in Fig. 1.

utility of straightforward linear modeling in quantitating the phenomena underlying in vivo hepatic uptake of tracer against an underlying steady state of bulk material. The finding that the labeled water curve is the appropriate reference for the labeled ethanol curve in these in vivo experiments indicates that the labeled water curve represents the outflow pattern that labeled ethanol would have had if there had been no metabolic sequestration process. The difference between the labeled water and labeled ethanol curves (illustrated in the upper panel of Fig. 16) therefore represents the effect of the metabolic sequestration process. Since the labeled water curve is the appropriate second reference for these labeled ethanol curves, the labeled ethanol outflow concentration per milliliter will be the product of the corresponding value for labeled water and the exponential of the negative value of the product of the rate constant and the sinusoidal transit time; hence, the uptake rate constant can be estimated in a fairly simple fashion by measuring the slope on a plot of the natural logarithm of the ratio of labeled water to labeled ethanol outflow fractions per milliliter versus time (this approach is illustrated in the lower panel of Fig. 16).

The lower part of Fig. 16 also provides a way of reexamining the assumptions underlying the analysis of individual experiments. In each set of experimental data the slope of the natural logarithm of the ratio versus time is constant. The damping function relating the labeled water and labeled alcohol curves is $\exp\{-(V_{tot}/[\hat{u} + K_m])(t - t_o)\}$. The rate constant $(V_{tot}/[\hat{u} + K_m])$ will be expected to be constant only if the $\hat{u}$ value corresponding to the various individual pathways does not change in significant fashion in relation to the K_m, from short transit time to long transit time pathways within the individual experiment. If a significant decrease with respect to the K_m does occur in the individual $\hat{u}$ values for the long transit time pathways, the damping effect along these would be larger than if the rate constant were unchanged, and an upward bowing of the ln ratio versus time plot would be expected. The lack of bowing from the beginning to the end of the experimental data indicates that a single $\hat{u}$ value (corresponding to the mixed venous outflow) is adequate to describe the set of data within an individual experiment.

Thus, in this data set the analysis of an individual experiment provides a way of accounting for input-output tracer relations, but it cannot be used to account for the overall saturation behavior of the sequestration process. The analysis at the level of the single experiment must be complemented by a way of unifying the events obtained at various plasma concentrations into a comprehensible whole. Both the accompanying work by Goresky et al. (19) and the theoretical analysis outlined by Bass et al. (1) indicate that the logarithmic average concentra-

tion is the mean concentration to which it is appropriate to relate the magnitude of the uptake process. This provides a way of using the experimental tracer uptake rate constant to estimate the V_{tot} and K_m parameters characterizing the enzymic disposal mechanism and implicitly takes into account the steady-state profile along the sinusoids.

Although this approach is appropriate and valid when the material concerned is entering the liver cells with no restrictions, the approach will not be valid if there is a restriction at the hepatocyte cell membrane (i.e., if a steady-state drop in concentration occurs across that membrane). Goresky et al. (17) have previously pointed out that, when a concentration drop occurs across the membrane, the concentrations relating to saturation phenomena at the level of metabolic sequestration processes are necessarily the intracellular concentrations. With substances for which the cell membranes constitute a significant barrier to passage, a different set of expressions are required, inasmuch as the concentration profile to which the uptake process must be related is that in the cells rather than in the sinusoids. An approach to this problem is outlined in a paper by Goresky et al. (19). The expression developed in that study for the intracellular uptake rate constant is analogous to that utilized in the present paper, but with the intracellular concentration effectively modulating the saturation of the uptake mechanism. It has the form $V_{tot}/(\hat{z} + K_m)$, where $\hat{z}$ is the logarithmic average intracellular concentration.

Comparison of our parameter estimates for ethanol removal system with those found by others. In general, the V_{tot} values derived from our in vivo studies are expected to be accurate. The V_{tot} value derived from our data is somewhat higher than those found by Keiding et al. (26) in their steady-state in vivo input-output concentration studies in pigs and humans after fasting for 48 and 12 h, respectively. Some of the difference may be consequent to the protocol we used, one in which dogs were not fasted for a prolonged period [prolonged starvation in the rat, for instance, has been found to decrease the maximal rate of ethanol oxidation to about 50% of that found in the fed state (24)]; some of the difference is undoubtedly due to our consideration of heterogeneity in the modeling [use of a single capillary model will be expected, on the basis of past analyses of heterogeneity, to result in a V_{tot} estimate that is too small (Refs. 14 and 38 and J. B. Bassingthwaighte and C. A. Goresky, unpublished observations)]; and finally some of the difference must be intrinsic to the difference in species.

The K_m values derived in the past for the removal process (by analysis of either intravenous disappearance curves or uptake by isolated perfused preparations) are generally too large, inasmuch as the removal process is usually related to input concentrations rather than the mean concentration at the removal site. The K_m values obtained by Keiding et al. (26) from their in vivo analysis of bulk hepatic removal of alcohol (0.27 mM in the pig and 0.14 mM for the human), which take into account steady-state concentration differences across the liver, are smaller than but generally of the same order of magnitude as the K_m value estimated for the removal process in our experiments on the dog (0.33 mM). The values correspond in general to the K_m of alcohol dehydrogenase, the principal ethanol-metabolizing mechanism, rather than to that of the microsomal ethanol-oxidizing system (29). We have not been able to find a K_m value describing the binding of ethanol to purified dog alcohol dehydrogenase for comparison. The K_m values found by in vitro analysis of either crude liver suspensions or purified alcohol dehydrogenase from other species vary somewhat and are expected to change with temperature, pH, ionic strength, and the nature of the buffer; thus, the values reported are expected only to approximate in vivo values. For the rat, Feytmans and Leighton (9) found a K_m of 0.26; Lundquist et al. (30), 0.3 mM; and Theorell et al. (41), 0.59 mM. Pietruszko et al. (35) found a K_m of 0.76 mM for the horse and Damgaard et al. (7) found a K_m of 1.5 mM for the pig, whereas Lange et al. (28) found a K_m of 2.7 mM at pH 10 and Pietruszko et al. (35) found a value of 0.40 mM at pH 7.5 for the human. This change in K_m with pH has also been observed in other species. The values reported above are generally those found at the more physiological pH. In an overall sense these values compare favorably with the K_m value that we found in the dog. There is a correspondence rather than a disparity between the in vivo and in vitro values.

Approach utilized to analyze tracer ethanol-bulk concentration interface. The approach developed here can be utilized wherever the substance being considered undergoes flow-limited distribution into the liver cells and removal from these cells. The approach takes into account both the lengthwise concentration profile that occurs along each sinusoid and the distribution of sinusoidal transit times (which accounts for both the characteristic forms of the outflow tracer dilution curves and the interrelations between these curves).

This approach has been applied in the steady state. Its formulations could be extended to deal with the nonsteady state represented by intravenous disappearance curves (10) if the probes being examined were distributed into the liver in a flow-limited fashion and if data were acquired in a form suitable for securing estimates of the characteristic parameters of the removal system. Any such modeling must now include the potential for describing the lengthwise sinusoidal concentration profiles. Compartmental analysis of the kind proposed by Dedrick and Forrester (8), in which this phenomenon is neglected, can no longer be considered either adequate or appropriate.

Flow-limited distribution of labeled alcohols in liver. Delayed wave flow-limited distribution characterizes both the distribution of labeled sucrose in the Disse space and the distribution of labeled water into the whole of the liver parenchyma. Labeled sucrose, which then marks the outflow pattern for a substance not entering the liver cells, emerges at the outlet substantially before labeled water, and its dilution profile reaches a substantially higher and earlier peak than does labeled water and decays more quickly (15). If the liver cell membrane presented any effective resistance to the entry of any one of the alcohols, a throughput or less delayed component to the curve would be expected, emerging at the outflow before the labeled water (or the appropriate flow-limited

reference) and pulling the upslope of the curve forward in time. No such effect was observed. All of the labeled alcohol curves are either coincident with the labeled water or are delayed in time with respect to the labeled water, in the manner expected for a flow-limited substance with a larger volume of distribution than labeled water. The data indicate that the labeled alcohols undergo flow-limited distribution into a space that in each case is as large as or larger than that available to labeled water. This in turn indicates that the permeability of the hepatocytes for the alcohols is at least as large as it is for labeled water. It is of interest to note that, in Novikoff hepatoma cells, the permeabilities of the cell membrane to all of the alcohols utilized in the present series of experiments have been found to be larger than those for labeled water (36).

When an injection mixture is preequilibrated prior to its introduction, red cell carriage of label (the trapping and translocation of label in the red cells) occurs when the permeability of the red cell membrane is low for the tracer. When the permeability of the red cells is large and there are no other barriers in the system, the curve approaches that for a label undergoing flow-limited distribution into both the red cells and its extravascular space (labeled water for the two shorter-chain-length alcohols). In a regime of high but slightly limiting red cell permeability, the label is pulled forward in time by carriage in the red cells (18). The upslope occurs earlier than that for the appropriate reference, the peak of the curve is somewhat flattened, and the downslope is somewhat prolonged (the mean transit time for the curve is identical to that for its appropriate reference). In the dog, the permeability of the liver parenchymal cells is in general larger than that of its red cells, and a red cell carriage effect is expected, rather than an effect at the parenchymal cell membrane, as the permeability of the probe molecule is gradually reduced. In the liver, the effect is barely visible when labeled urea is utilized (18). The tracer permeability of dog erythrocytes to urea at 20°C is 55×10^{-5} cm·s^{-1} and, at 37°C, 117×10^{-5} cm·s^{-1} (11). The dog red cell permeabilities to all of the alcohols utilized in the present study are substantially larger than this value (12) and, except for methanol and ethanol, are larger than the value for labeled water [569×10^{-5} cm·s^{-1} at 20°C (37) and 908×10^{-5} cm·s^{-1} at 37°C (13)]. The membrane-plasma partitioning of the alcohols into the red cell membranes is not so high [for the series utilized, a maximum of 3.2 for pentanol (39)] that an additional phase effect would be expected for the red cells by virtue of carriage of the label in the red cell membrane.

The results of our present studies can be used with the modern data on red cell permeability to interpret the multiple-indicator dilution studies carried out by Chinard et al. (4) in order to examine the behavior of the monohydric straight-chain alcohols in the kidney. In their studies, these investigators found precession on the upslope of the dilution curves of the alcohols with respect to labeled water, increasing from methanol to hexanol. The precession presents a problem. In terms of the phenomena encountered in the liver, it could occur either because the renal parenchymal cells are substantially less permeable to the labeled alcohol than to labeled water (this appears unlikely, although it is possible) or because of red cell carriage of label. The phenomena observed would be expected only if the tracer permeability of the red cells for these alcohols becomes substantially smaller than that for labeled water with increase in chain length, and the data of Garrick et al. (12) show that this does not happen. The lack of evidence for longitudinal diffusion in the liver, where these effects would be expected to be enhanced relative to the kidney because the transit times are larger and velocities of flow smaller than in kidney, indicates that the axial diffusion mechanism proposed by Perl et al. (33) cannot account for the data either. The microcirculation in the liver has a structure such that large-scale diffusion fluxes between entering and leaving vessels will not occur, independent of carriage by flow (input and output sites are separated in space in a quasi-crystalline type of array), whereas in the kidney there is a looping countercurrent type of postglomerular microcirculation, with input and output sites apposed in space. It therefore appears likely that countercurrent shunting of labeled alcohol from input to output (perhaps because of a higher permeability of these cells to the alcohols than to water) underlies the form of the outflow dilution curves that these authors have observed. Despite this hypothesized explanation, it is obvious that the problem needs further examination. There is still uncertainty concerning the basis for the differing behavior of the monohydric alcohols in the liver and the kidney.

Correspondence of our in vivo K_m estimates for series of monohydric primary alcohols with those obtained from in vitro observations. We have been unable to find estimates for the K_m values of dog alcohol dehydrogenase for the straight-chain monohydric alcohols determined in vitro, but values for other species have been found and are listed in Table 5. The values of the enzyme K_m for the various alcohols in other species determined in vitro tend to bracket those arising from our in vivo experiments, and thus our K_m values appear sensible in terms of their order of magnitude. An overall trend is apparent in the in vivo observations, corresponding to the in vitro observations. The K_m values tend to diminish with increase in the chain length of the alcohol.

Generality of our description of an enzymic space effect. The description that we have developed corresponds to both the phenomena explored experimentally in our present work (the extra space evident when trace amounts of material are introduced into a system with no bulk carrier and its virtual disappearance when there are high levels of carrier substrate) and to the observations outlined in the introduction section, which were encountered in earlier experiments: the expansion of the intracellular space available to tracer bilirubin with increase in ligandin concentration, when no carrier is present in the system, and the decrease in the hepatic intracellular space available to labeled fatty acids, when the binding sites on Z protein are occupied by the infusion of bulk amounts of their brominated analogues.

One additional large area in which this approach promises to be of particular utility is in the quantitative description of binding to receptors in vivo, when the concentration of the agonist varies around the range of the K_m of the receptor. In this situation tracer techniques

may well permit derivation of an estimate of the K_m of the binding site on the receptor (6).

We express our appreciation to Louise Gagnon, Laurie-Ellen Gwynne, and Kim McMillan for their excellent technical assistance; to Heidi Greschner for typing the manuscript; and to the Medical Research Council of Canada, the Quebec Heart Foundation, the Edwards Foundation, and the Department of Medicine of the Montreal General Hospital for their financial support.

C. A. Goresky is the recipient of a Career Investigator Award from the Medical Research Council of Canada.

Address for reprint requests: C. A. Goresky, University Medical Clinic, Montreal General Hospital, 1650 Cedar Ave., Montreal, Quebec H3G 1A4, Canada.

Received 11 December 1980; accepted in final form 13 August 1982.

REFERENCES

1. BASS, L., S. KEIDING, K. WINKLER, AND N. TYGSTRUP. Enzymatic elimination of substrates flowing through the intact liver. *J. Theor. Biol.* 61: 393–409, 1976.
2. BONNICHSEN, R. Ethanol: determination with alcohol dehydrogenase and DPN. In: *Methods of Enzymatic Analysis*, edited by H.-U. Bergmeyer. New York: Academic, 1963, p. 285–287.
3. CHINARD, F. P., R. EFFROS, W. PERL, AND M. SILVERMAN. Organ vascular and extravascular compartments in vivo. In: *Compartments, Pools, and Spaces in Medical Physiology*, edited by P.-E. Bergner, C. C. Lushbaugh, and E. B. Anderson. Oak Ridge, TN: US Atomic Energy Commission, 1967, p. 381–422.
4. CHINARD, F. P., C. N. THAW, A. C. DELEA, AND W. PERL. Intrarenal volumes of distribution and relative diffusion coefficients of monohydric alcohols. *Circ. Res.* 25: 343–357, 1969.
5. CHINARD, F. P., G. J. VOSBURGH, AND T. ENNS. Transcapillary exchange of water and other substances in certain organs of the dog. *Am. J. Physiol.* 183: 221–234, 1955.
6. COUSINEAU, D., C. P. ROSE, AND C. A. GORESKY. In vivo characterization of the adrenergic receptors in the working canine heart. *Circ. Res.* 49: 501–510, 1981.
7. DAMGAARD, S. E., L. SESTOFT, F. LUNDQUIST, AND N. TYGSTRUP. The interrelationship between fructose and ethanol metabolism in the isolated perfused pig liver. *Acta Med. Scand. Suppl.* 542: 131–140, 1972.
8. DEDRICK, R. L., AND D. D. FORRESTER. Blood flow limitations in interpreting Michaelis constants for ethanol oxidation in vivo. *Biochem. Biopharmacol.* 22: 1133–1140, 1973.
9. FEYTMANS, E., AND F. LEIGHTON. Effects of pyrazole and 3-amino-1,2,4-triazole on methanol and ethanol metabolism in the rat. *Biochem. Pharmacol.* 22: 349–360, 1973.
10. FORKER, E. L., AND B. LUXON. Hepatic transport kinetics and plasma disappearance curves: distributed modeling versus the conventional approach. *Am. J. Physiol.* 235 (*Endocrinol. Metab. Gastrointest. Physiol.* 4): E648–E660, 1978.
11. GARRICK, R. A., AND F. P. CHINARD. Permeability of dog erythrocytes to ^{14}C-urea. *Microvasc. Res.* 20: 88–91, 1980.
12. GARRICK, R. A., B. C. PATEL, AND F. P. CHINARD. Permeability of dog erythrocytes to lipophilic molecules: solubility and volume effects. *Am. J. Physiol.* 238 (*Cell Physiol.* 7): C107–C113, 1980.
13. GARRICK, R. A., B. C. PATEL, AND F. P. CHINARD. Erythrocyte permeability to lipophilic solutes: changes with temperature. *Am. J. Physiol.* 242 (*Cell Physiol.* 11): C74–C80, 1982.
14. GONZALEZ-FERNANDEZ, J. M., AND S. E. ATTA. Maximal substrate transport in capillary networks. *Microvasc. Res.* 5: 180–198, 1973.
15. GORESKY, C. A. A linear method for determining liver sinusoidal and extravascular volumes. *Am. J. Physiol.* 204: 626–640, 1963.
16. GORESKY, C. A., G. G. BACH, AND B. E. NADEAU. On the uptake of materials by the intact liver: the concentrative transport of rubidium-86. *J. Clin. Invest.* 52: 975–990, 1973.
17. GORESKY, C. A., G. G. BACH, AND B. E. NADEAU. On the uptake of materials by the intact liver: the transport and net removal of galactose. *J. Clin. Invest.* 52: 991–1008, 1973.
18. GORESKY, C. A., G. G. BACH, AND B. E. NADEAU. Red cell carriage of label: its limiting effect on the exchange of materials in the liver. *Circ. Res.* 36: 328–351, 1975.
19. GORESKY, C. A., G. G. BACH, AND C. P. ROSE. Effects of saturating metabolic uptake on space profiles and tracer kinetics. *Am. J. Physiol.* 244 (*Gastrointest. Liver Physiol.* 7): G215–G232, 1983.
20. GORESKY, C. A., D. S. DALY, S. MISHKIN, AND I. M. ARIAS. Uptake of labeled palmitate by the intact liver: role of intracellular binding sites. *Am. J. Physiol.* 234 (*Endocrinol. Metab. Gastrointest. Physiol.* 3): E542–E553, 1978.
21. GORESKY, C. A., AND B. E. NADEAU. Uptake of materials by the intact liver: the exchange of glucose across the cell membrane. *J. Clin. Invest.* 53: 634–646, 1974.
22. GORESKY, C. A., AND M. SILVERMAN. Effect of correction of catheter distortion on calculated sinusoidal blood volumes. *Am. J. Physiol.* 207: 883–892, 1964.
23. GORESKY, C. A., W. H. ZIEGLER, AND G. G. BACH. Capillary exchange modeling: barrier-limited and flow-limited distribution. *Circ. Res.* 27: 739–764, 1970.
24. HIGGINS, J. J. Control of ethanol oxidation and its interaction with other metabolic systems. In: *Biochemistry and Pharmacology of Ethanol*, edited by E. Majchrowicz and E. Noble. New York: Plenum, 1979, vol. 1, p. 249–351.
25. JOHANSEN, S., AND S. KEIDING. A family of models for the elimination of substrate by the liver. *J. Theor. Biol.* 89: 549–556, 1981.
26. KEIDING, S., S. JOHANSEN, I. MIDTBOLL, A. ROBOL, AND L. CHRISTIANSEN. Ethanol elimination kinetics in human liver and pig liver in vivo. *Am. J. Physiol.* 237 (*Endocrinol. Metab. Gastrointest. Physiol.* 6): E316–E324, 1979.
27. KEIDING, S., S. JOHANSEN, K. WINKLER, D. TONNENSEN, AND N. TYGSTRUP. Michaelis-Menten kinetics of galactose elimination by the isolated pig liver. *Am. J. Physiol.* 230: 1302–1313, 1976.
28. LANGE, L. G., A. J. SYTKOWSKI, AND B. L. VALLEE. Human liver alcohol dehydrogenase: purification, composition, and catalytic features. *Biochemistry* 15: 4687–4693, 1976.
29. LIEBER, C. S., AND L. M. DECARLI. Hepatic microsomal ethanol-oxidizing system. *J. Biol. Chem.* 245: 2505–2512, 1970.
30. LUNDQUIST, F., I. SVENDSEN, AND P. HYLTOFT-PETERSEN. The metabolism of ethanol in rat-liver suspensions. *Biochem. J.* 86: 119–124, 1963.
31. LUNDQUIST, F., AND H. WOLTHERS. The kinetics of alcohol elimination in man. *Acta Pharmacol. Toxicol.* 14: 265–289, 1958.
32. LUNDSGAARD, E. Alcohol oxidation as a function of the liver. *CR Trav. Lab. Carlsberg Ser. Chim.* 22: 333–337, 1938.
33. PERL, W., AND F. P. CHINARD. A convection-diffusion model of indicator transport through an organ. *Circ. Res.* 27: 273–298, 1968.
34. PIETRUSZKO, R. Nonethanol substrates of alcohol dehydrogenase. In: *Biochemistry and Pharmacology of Ethanol*, edited by E. Majchrowicz and E. Noble. New York: Plenum, 1979, vol. 1, p. 88–106.
35. PIETRUSZKO, R., K. CRAWFORD, AND D. LESTER. Comparison of substrate specificity of alcohol dehydrogenases from human liver, horse liver, and yeast towards saturated and 2-enoic alcohols and aldehydes. *Arch. Biochem. Biophys.* 159: 50–60, 1973.
36. POLEFKA, T. G., W. G. REDWOOD, R. A. GARRICK, AND F. P. CHINARD. Permeability of Novikoff hepatoma cells to water and monohydric alcohols. *Biochim. Biophys. Acta* 642: 67–78, 1981.
37. REDWOOD, W. R., E. RALL, AND W. PERL. Red cell permeability deduced from bulk diffusion coefficients. *J. Gen. Physiol.* 64: 706–729, 1974.
38. ROSE, C. P., AND C. A. GORESKY. Vasomotor control of capillary transit time heterogeneity in the canine coronary circulation. *Circ. Res.* 39: 541–554, 1976.
39. SEEMAN, P., S. ROTH, AND H. SCHNEIDER. The membrane concentrations of alcohol anesthetics. *Biochim. Biophys. Acta* 225: 171–184, 1971.
40. STURTEVANT, F. M., AND R. P. STURTEVANT. Chronopharmacokinetics of ethanol. In: *Biochemistry and Pharmacology of Ethanol*, edited by E. Majchrowicz and E. Noble. New York: Plenum, 1979, p. 27–40.
41. THEORELL, H., A. NYGAARD, AND R. BONNICHSEN. Studies on liver alcohol dehydrogenase. III. The influence of pH and some anions on reaction velocity constants. *Acta Chem. Scand.* 9: 1148–1165, 1955.
42. TSAI, C. S. Relative reactivities of primary alcohols as substrates of liver alcohol dehydrogenase. *Can. J. Biochem.* 46: 381–385, 1968.
43. WOLKOFF, A. W., C. A. GORESKY, J. SELLIN, Z. GATMAITAN, AND I. M. ARIAS. Role of ligandin in transfer of bilirubin from plasma into liver. *Am. J. Physiol.* 236 (*Endocrinol. Metab. Gastrointest. Physiol.* 5): E638–E648, 1979.